Kragujevac J. Sci. (2025) 47 (1) 29-44
doi: 10.5937/KgJSci2501029P

UDC 544.522.143:544.538:537.12
Original scientific paper

FEMTOSECOND LASER-INDUCED BREAKDOWN IN WATER-LIKE TISSUES: INFLUENCE OF WAVELENGTH AND PULSE DURATION ON ELECTRON DYNAMICS

Violeta Petrović[1], Hristina Delibašić Marković[1,] *, Ivan Petrović[2]

[1] *University of Kragujevac, Faculty of Science, Radoja Domanovića 12, 34000 Kragujevac, Republic of Serbia*
[2] *Academy of Professional Studies Šumadija, Department in Kragujevac, Kosovska 8, 34000 Kragujevac, Republic of Serbia Serbia*
*****Corresponding author; E-mail: hristina.delibasic@pmf.kg.ac.rs

(Received March 03, 2025; Accepted May 30, 2025)

ABSTRACT. This study explores the initiation mechanisms of laser-induced breakdown in water-like tissues by examining the impact of ultra-short laser pulses at varying wavelengths. Using numerical simulations, we analyse the electron dynamics triggered by pulse durations from 1 fs to 150 fs at two specific wavelengths, 400 nm and 800 nm. The results highlight how shorter pulses predominantly drive photoionization due to their intense peak powers, while longer pulses facilitate cascade ionization, enhancing electron densities through prolonged interactions with the tissue. Our analysis reveals that the deeper penetration of 800 nm pulses allows for more significant cascade ionization effects, particularly at extended pulse durations, leading to a substantial increase in electron density. This study underscores the role of pulse duration and wavelength in influencing the primary ionization processes essential for laser induced breakdown, providing a foundation for optimizing laser applications in medical and material sciences.

Keywords: laser induced breakdown, photoionization, Keldysh parameter, free-electron density.

INTRODUCTION

The nonlinear optical characteristics of liquid water are essential in numerous scientific fields, especially in investigations into the interaction of laser pulses with water-rich tissues, including the human eye, skin, and brain (LINZ *et al.*, 2016; HAN *et al.*, 2015; SALEHI *et al.*, 2020). High-intensity laser pulses cause nonlinear optical events in different samples including the Kerr effect (YANG *et al.,* 2024) and self-focusing (NUZZO *et al.,* 2010). The Kerr effect results in variations in the refractive index of the sample with respect to light intensity;

ORCID ID:
V. Petrović - 0000-0002-7865-523X; H. Delibašić Marković- 0000-0002-8391-4179;
I. Petrović- 0009-0003-2419-8787.

therefore, altering the propagation path of the light. When the change in refractive index that depends on intensity causes a lensing effect within the material, it leads to self-focusing. This happens because the laser light is concentrated into a smaller area, which further boosts its intensity. This intense concentration of energy can lead to laser-induced breakdown (LIB), a process where the energy is so high that it ionizes the atoms and molecules, creating a dense plasma of electrons and ions. By absorbing and propagating the arriving laser light, this plasma plays a part in laser-tissue interaction since it shields underlying tissues from thermal and photomechanical damage.

Over the years, the perspective on LIB in water-like tissues has been thoroughly developed, notably the relationship between pulse duration and intensity (FANG AND HU, 2004; WEN *et al.* 2019; DELIBASIC *et al.* 2021). This study revealed new insights into the dynamics that drive LIB and its applications in ocular surgery and precision tissue ablation over the nanosecond (ns) to ultrashort femtosecond (fs) time scales. Shorter pulse durations have been shown to lower the breakdown threshold, altering the physical mechanics of plasma production and, as a result, plasma dynamics. For example, HAMMER *et al.* (1996) demonstrated how the shielding efficacy of LIB changes with pulse duration; efficiency declines from nanoseconds to 300 fs but increases when pulses are reduced to 125 fs. Furthermore, SARAPE-TUDORAN *et al.* (2006) investigated the ultrashort domain utilizing spectrally resolved reflection spectroscopy and transient imaging techniques to detect early breakdown events at water surfaces induced by fs pulses. They gave significant insights into plasma dynamics, such as the delay before plasma expansion and transient electron density, which are required to understand and optimize LIB operations. In addition, SCHAUFF *et al.* (2006) used time-resolved imaging to study LIB dynamics in water at eight-order-of-magnitude time scales (microseconds (µs) to fs), making important contributions. Their findings were essential in understanding early picosecond (ps) plasma dynamics, revealing a delay of around 220 fs before plasma expansion, which they attributed to electron-ion energy transfer. These findings, when taken together, highlight the importance of pulse length in LIB in water-like tissues. Shorter pulse lengths not only reduce the breakdown threshold, but they also have a significant impact on plasma dynamics; each pulse range offers unique choices for LIB process management. These findings provide the foundation for our current research, which focuses on pulse durations ranging from 1 to 150 fs.

In this work, we simulate how various pulse lengths influence the primary ionization processes - namely, photoionization (PI) and cascade ionization (CI) using a numerical method that models the optical characteristics of water-like tissues. Our primary focus is on understanding these fundamental ionization mechanisms, to clearly capture the evolution of free-electron density under ultrashort laser pulse irradiation. While other effects such as thermal dynamics, tissue heterogeneity, and nonlinear phenomena play important roles in laser-tissue interactions, especially for longer pulses, these involve complex coupled processes like heat diffusion and hydrodynamic responses that are beyond the current model's scope. By limiting the study to a homogeneous, water-like medium and focusing on core ionization dynamics, we aim to provide a clear and computationally feasible foundation. These considerations enable us to analyse how the dominant ionization mechanisms vary with pulse duration, revealing different interaction regimes. Because of their small interaction periods and strong peak strengths, the interaction for the shorter pulses in our study is mostly driven by PI up to 50 fs. Though their multiplication is constrained by the short pulse duration, the electrons produced during this phase are essential since they form seeds for any later CI. The dynamics drastically change as we increase the pulse duration to 150 fs. The initially few seed electrons have adequate time to multiply via CI. This mechanism greatly raises the electron density, which produces a more noticeable LIB effect. Studies of other transparent materials have also shown similar findings whereby longer pulse durations cause a notable rise in electron density owing to CI (HAMMER *et al.,* 1996; CHRISTENSEN and BALLING, 2009; LINZ *et al.,* 2025). We present a study of how ultrashort pulse durations affect the nonlinear optical characteristics of water-

like tissues by merging findings from our numerical simulations with available experimental data.

The rest of the paper is structured as follows: a theoretical study of the LIB model under investigation is given in Section 2. Examining both, the mechanisms of free-electron density generation and its dissipation, this part addresses the fundamental ideas of laser-induced plasma (LIP) generation in water-like tissues by fs lasers. Here we also describe the numerical technique used to solve the rate equations that govern free electron density. The results are reported in Section 3, along with a comparison of electron densities produced by various laser pulse lengths and intensities. Section 4 summarizes the key findings and conclusions of this study.

THEORETICAL FRAMEWORK

Intense electromagnetic radiation fields and electrons in a medium that mimic water-like tissues, like the human eye, skin, and brain (HAN *et al.*, 2015; LINZ *et al.*, 2016; SALEHI *et al.*, 2020), are the subject of this study's theoretical framework. The ionization potential of these tissues, which are mostly made of water, is usually greater than the energy of the interacting photons. This physical property makes it easier for nonlinear PI processes to produce quasi-free electrons in the conduction band. After these free charges are produced, they can absorb more kinetic energy from the electric field by a process known as inverse bremsstrahlung (IB). The generation of additional free carriers through impact ionization depends on this energy gain. Since water molecules primarily interact with laser pulses, the high-water content in these tissues supports our models' characterization of them as water-like media (LINZ *et al.*, 2016; HAN *et al.*, 2015; SALEHI *et al.*, 2020). The quick accumulation of free carriers brought on by this interaction causes the medium to ionize quickly, plasma to develop, and the medium's absorption coefficient to rise significantly. The quick energy transmission from the laser to the medium depends on this increased absorption coefficient. When the free electron density above a critical threshold, usually between $10^{18} - 10^{20}\mathrm{cm}^{-3}$, the phenomena is categorized as LIB (SACCHI, 1991). The plasma is sufficiently dense at this level to successfully shield the underlying tissue by absorbing a sizable amount of the input laser energy.

We use a rate equation that quantitatively characterizes the temporal evolution of free electron density, ρ, in response to laser irradiation to efficiently represent the dynamic process of LIB in water-like tissues. Understanding the complex interactions between generation and loss mechanisms that control the behavior of plasma in these tissues depends on this equation. The expression for the rate equation is (KENNEDY, 1995):

$$\frac{d\rho}{dt} = W_{PI} + W_{CI} \cdot \rho - W_R \cdot \rho. \tag{1}$$

The main goal is to understand the influences of fs pulse length on the primary ionization mechanisms of water-like tissues, specifically by looking at photoionization, W_{PI}, and cascade ionization, W_{CI}, rates. We employ a numerical method specifically designed to describe the light transport in tissues that exhibit similar properties to water. Note that our model has an additional term, W_R, which quantifies the effective relaxation time as $W_R = T^{-1}$, where T represents the relaxation time calculated to be 2 ps (LINZ *et al.*, 2016). This term is crucial for accurately modeling the decay dynamics of the plasma generated by laser pulses ranging from 1 fs to 150 fs at wavelengths of 400 nm and 800 nm. By integrating this term, we enhance our model's ability to simulate how quickly the plasma dissipates post-irradiation, a critical factor in understanding the overall energy dynamics within the tissue. The knowledge of both creations, W_{PI} and W_{CI}, and loss, W_R, processes inside the LIP is important since it helps us to determine the conditions under which each ionization phenomena predominates.

Furthermore, it is essential to consider the influence of laser intensity, I, on the temporal evolution of free-electron density, $\rho = \rho(t)$, which directly reflects the energy absorbed by the tissue. By modeling the laser pulse intensity with a Gaussian profile, $I(t) = I_0 \exp(-4\ln 2 t^2/\tau^2)$ (I_0 is the peak intensity of the laser pulse and τ is the full width at half maximum (FWHM) of the intensity profile) (GRUZDEV, 2014), we can effectively replicate realistic medical laser operation conditions. This modeling choice reflects the actual behaviour of laser systems, where the intensity typically follows a Gaussian distribution over time. The evolution of $\rho(t)$ modeled under these conditions provides insights into how variations in pulse length and intensity influence the rate of electron generation and the subsequent saturation point (see (HAMAM and GAMAL, 2018; DELIBASIC *et al.*, 2020)). This saturation, indicative of a balance between electron generation and loss mechanisms, underscores the complex interplay that must be managed to optimize laser parameters effectively.

Photoionization rate

PI is a critical process in the study of optical breakdown, where the interaction of intense laser pulses with matter results in the ejection of electrons from their atomic or molecular orbitals. This process is fundamental to initiating plasma formation, setting the stage for various optical phenomena that characterize LIB. In laser physics, the mechanism and efficiency of PI depend on the interplay between the laser's properties and the material's characteristics, influencing how energy is transferred from the laser to the material. The complexities of PI are captured by the Keldysh gamma parameter, γ, which is a dimensionless quantity that helps to predict the dominant ionization mechanism under specific laser irradiation conditions. It is defined as (KELDYSH, 1964):

$$\gamma = \frac{\omega\sqrt{2I_p}}{F}, \tag{2}$$

where ω is the angular frequency, I_p is the ionization potential, and F is the amplitude of the electric field of laser radiation, given by: $F = \sqrt{2I/cn\varepsilon_0}$. Here, I represents the peak laser intensity, n the refractive index of the material, c is the speed of light in vacuum, $c = 3 \times 10^8$ m/s, and ε_0 is the permittivity of free space, $\varepsilon_0 = 8.85 \times 10^{-12}$ F/m. The index n is particularly important as it varies with the wavelength of the laser, λ, and the specific material properties, $n = n(\lambda)$. It can be calculated using the Sellmeier dispersion formula (BERGE, 1984): $n = \sqrt{1 + \left[A_1\lambda^2/\left(\lambda^2 - {B_1}^2\right)\right] + \left[A_2\lambda^2/\left(\lambda^2 - {B_2}^2\right)\right] + \left[A_3\lambda^2/\left(\lambda^2 - {B_3}^2\right)\right]}$ (here, $A_{1,2,3}$ and $B_{1,2,3}$ are the coefficients, which are experimentally determined for different materials (https://refractiveindex.info/). The significance of γ parameter lies in its ability to delineate between different PI regimes - multiphoton ionization (MPI) and tunnel ionization (TI). When $\gamma \gg 1$, MPI dominates, where several low-energy photons are required to eject an electron. Conversely, when $\gamma \ll 1$, TI is predominant, characterized by an electron tunneling through the potential barrier lowered by the strong electric field of the laser. The intermediate regime, $\gamma \approx 1$, is of particular importance because it signifies a condition under which the characteristics of both MPI and TI can influence the ionization process. This regime is sensitive to the precise configuration of the laser pulse, including its intensity, duration, and frequency, as well as the material's ionization potential and electronic structure. Understanding this regime is crucial because the behaviour of the LIP in this regime can lead to unique and sometimes unpredictable effects due to the competing influences of MPI and TI, which can drastically affect the efficiency and outcome of the laser interaction. Therefore, modeling the PI rate across the entire spectrum of γ and I values is crucial for a thorough comprehension of LIB, facilitating the creation of more precise predictive models adaptable to diverse applications (WANG *et al.*, 2023).

Building on the foundational rate equation for LIB in water-like tissues (see Eq. (1)), we delve into the specific mechanisms of ionization, particularly focusing on the PI rate, W_{PI}. The PI rate is given by the following expression (KELDYSH, 1964):

$$W_{PI} = \frac{2\omega}{9\pi}\left(\sqrt{\frac{m_e\omega}{\hbar}}\right)^3 \mathcal{Q}\left(\gamma, \frac{I_p^*}{\hbar\omega}\right) \exp\left[-\pi\eta^* \frac{\{K(\gamma_1)-E(\gamma_1)\}}{E(\gamma_2)}\right]. \quad (2)$$

In this equation, m_e is the effective electron mass for water-like tissues, calculated as: $m_e = 1.2\, m_e^0$, where m_e^0 is the electron's rest mass, $m_e^0 = 9.11 \times 10^{-31}$ kg, and $\hbar$ denotes the reduced Planck constant, $\hbar = 1.054 \times 10^{-34}$ J · s. The function $\mathcal{Q}\left(\gamma, I_p^*/\hbar\omega\right)$, defined in the Eq. (2) is important as it dynamically adjusts the ionization probability in response to the Keldysh γ parameter, thus tailoring the model to the specific laser-material interaction parameters. It is defined as follows:

$$\mathcal{Q}\left(\gamma, \frac{I_p^*}{\hbar\omega}\right) = \sqrt{\frac{\pi}{2K(\gamma_2)}} \sum_{k=0}^{\infty} \exp\left[-\pi \frac{\{K(\gamma_1)-E(\gamma_1)\}n}{E(\gamma_2)}\right] \phi\left[\sqrt{\frac{\pi^2\left(2\eta^* - 2\frac{I_p^*}{\hbar\omega} + k\right)}{2K(\gamma_2)E(\gamma_2)}}\right]. \quad (3)$$

where I_p^* is the effective ionization potential, calculated as: $I_p^* = 2E(\gamma_2)I_p/\pi\gamma_1$. Here, I_p is the unperturbed ionization potential for water-like tissues, set at 6.5 eV (VOGEL AND NOACK, 2001). Additionally, η^* represents a dimensionless parameter, formulated as: $\eta^* = \langle I_p^*/\hbar\omega + 1\rangle$, which adjusts the integer party of the ionization potential relative to the photon energy of the laser. Furthermore, the complete elliptic integrals of the first, $K(\gamma_1)$ and $K(\gamma_2)$, and second, $E(\gamma_1)$ and $E(\gamma_2)$, kinds are calculated at modified γ values, where $\gamma_1 = \gamma/\sqrt{1+\gamma^2}$ and $\gamma_2 = 1/\sqrt{1+\gamma^2}$. Lastly, $\phi[\ldots]$ represents the Dawson probability integral which can be calculated using the following expression: $\phi[z] = \int_0^z \exp[y^2 - z^2]dy$.

In the study of LIB, a thorough understanding of the dynamics of free electron density is essential. This is particularly relevant when dealing with intense laser interactions in water-like tissues, where the full numerical solution of the photoionization rate W_{PI} provided by Eq. (2) offers a more detailed perspective. However, in many practical applications, researchers often simplify this complex interaction by employing analytical formulas tailored to specific ionization regimes, primarily TI and MPI (BLOEMBERGEN, 1974; HAMAM AND GAMAL, 2018). In the TI regime, the ionization process is dominated by the electron tunneling through a potential barrier, which is significantly distorted by the electric field of the laser. Under circumstances where $\gamma \ll 1$, the analytical expression for the TI rate accurately represents the quantum mechanical tunneling probability and is an exact approximation of Eq. (2). This formula effectively eliminates any contributions from MPI by isolating the TI mechanism, which is distinguished by its exponential dependency on the inverse of the electric field strength as (KELDYSH, 1964):

$$W_{TI} = \frac{2}{9\pi^2}\frac{I_p}{\hbar}\left(\frac{m_e I_p}{\hbar^2}\right)^{3/2}\left(\frac{e\hbar F}{\sqrt{m_e {I_p}^3}}\right)^{5/2} \exp\left[-\frac{\pi}{2}\frac{\sqrt{m_e {I_p}^3}}{e\hbar F}\left(1 - \frac{m_e\omega^2 I_p}{8e^2F^2}\right)\right]. \quad (4)$$

Here, e represents the electron charge, $e = 1.602 \times 10^{-19}$ C, and π is mathematical constant, $\pi = 3.14159\ldots$ On the other hand, as previously stated, MPI becomes the dominant mechanism in scenarios where electrons absorb multiple photons to accumulate enough energy to surpass the ionization potential. As a specialized case derived from Eq. (2) when $\gamma \gg 1$, MPI is characterized by its reliance on the high photon density, which directly influences the rate at which ionization occurs and can be defined as (KELDYSH, 1964):

$$W_{MPI} = \frac{2}{9\pi}\omega\left(\frac{m_e\omega}{\hbar}\right)^{3/2}\phi\left[\sqrt{2\left(\frac{I_p}{\hbar\omega}+1\right)-\frac{2I_p}{\hbar\omega}}\right]\left(\frac{e^2F^2}{16m_e\omega^2I_p}\right)^{\frac{I_p}{\hbar\omega}+1}\times$$
$$\times\exp\left[2\left(\frac{I_p}{\hbar\omega}+1\right)\left(1-\frac{e^2F^2}{4m_e\omega^2I_p}\right)\right]. \quad (5)$$

While the analytical models presented with Eqs. (4) and (5) provide a simplified view that is computationally less intensive and sufficient for extremities of the γ spectrum, they fall short in the intermediate regime, $\gamma \approx 1$. In this transition zone, both tunneling and photon absorption processes influence electron dynamics, leading to ionization characteristics that are not adequately captured by either TI or MPI models alone. This intermediate regime is important because it influences the threshold and stability of plasma generation - key determinants in the precision and efficiency of applications ranging from micron-scale material processing to targeted medical procedures using fs lasers. The overlapping of TI and MPI in this regime often triggers complex ionization dynamics such as ionization cascade, where initial ionization events catalyse further ionization, leading to rapid increases in free-electron density. These dynamics are crucial in fs laser applications due to the ultra-short pulse durations and high peak intensities, which uniquely position them at the cusp of these ionization mechanisms. Building on the discussion of the intermediate regime, $\gamma \approx 1$, Fig. 1 provides a detailed comparative analysis across two distinct laser wavelengths - 400 nm and 800 nm. This figure illustrates the PI (Eq. (2)), TI (Eq. (4)), and MPI (Eq. (5)) rates, showcasing how each ionization process responds under varied conditions of Keldysh gamma parameter, $0.01 \leq \gamma \leq 8.0$, and laser intensity, $1 \times 10^{12}\ \mathrm{W/cm^2} \leq I \leq 1 \times 10^{15}\ \mathrm{W/cm^2}$. Specifically, panels (a) and (c) explore the dynamics at 400 nm, while panels (b) and (d) focus on the 800 nm wavelength. In Figs. 1(a) and 1(b), the ionization dynamics are illustrated as functions of the γ parameter, offering insights into the relative impact of electric fields versus photon energy on electron behaviour. As γ increases - indicative of decreasing electric field strength relative to photon energy - a clear transition from TI to MPI is observed. The dashed lines represent TI rates, which dominate at lower γ values where the electric field is sufficiently strong to distort the potential barrier, thus facilitating electron tunneling. This phenomenon is consistent with the quantum mechanical description of tunneling where a strong electric field can significantly lower the potential barrier (KELDYSH, 1964; DELIBASIC *et al.*, 2018). Conversely, the dotted lines indicate MPI rates that increase as γ becomes larger. This shift highlights scenarios where electrons require the absorption of multiple photons to achieve the energy necessary to escape the atomic or molecular potential, a process well described by Keldysh theory (KELDYSH, 1964). The intersection of TI and MPI rates around γ values of 1.3 for 400 nm and 1.5 for 800 nm marks the intermediate regime. This is in accordance with the results presented in (FU *et al.*, 2012; WANG *et al.*, 2019). Described regime, where both TI and MPI significantly contribute to the ionization process, is critical because it represents a complex interplay where neither mechanism is solely dominant, leading to an understanding of laser-matter interaction under these conditions. Transitioning to Figs. 1(c) and 1(d), we examine how ionization rates scale with laser intensity, I, for both wavelengths. These figures demonstrate the nonlinear behaviours of ionization phenomena: TI rates increase with higher intensity, underscoring the enhanced efficiency of electric field-driven ionization under high-intensity conditions, where the field's influence on the potential barrier significantly aids in electron tunneling through the barrier. On the other hand, MPI rates decrease as intensity increases, reflecting their reduced effectiveness when the electric field becomes too strong, disrupting the absorption of multiple photons necessary for MPI. These observations align with the theoretical predictions (KELDYSH, 1964; POPOV, 2004), which suggest that at high photon densities and lower electric fields, MPI becomes more efficient than TI. As such, considering the full PI rate (see Eq. (2)), which incorporates both TI and MPI, becomes essential in models of free-electron density, especially in the fs laser pulse regime (YANG *et al.,* 2023). Incorporating the complete PI rate

into theoretical models allows for a comprehensive description of the initiation processes of free-electron generation, critical for accurately simulating and predicting laser-tissue interactions in medical and technological applications (SAJJADI *et al.,* 2013). This approach is supported by studies in the field (DU *et al.,* 1994; PETROVIĆ AND DELIBAŠIĆ, 2019), which emphasize the necessity of integrating both TI and MPI to fully capture the dynamics of ionization under varied laser parameters.

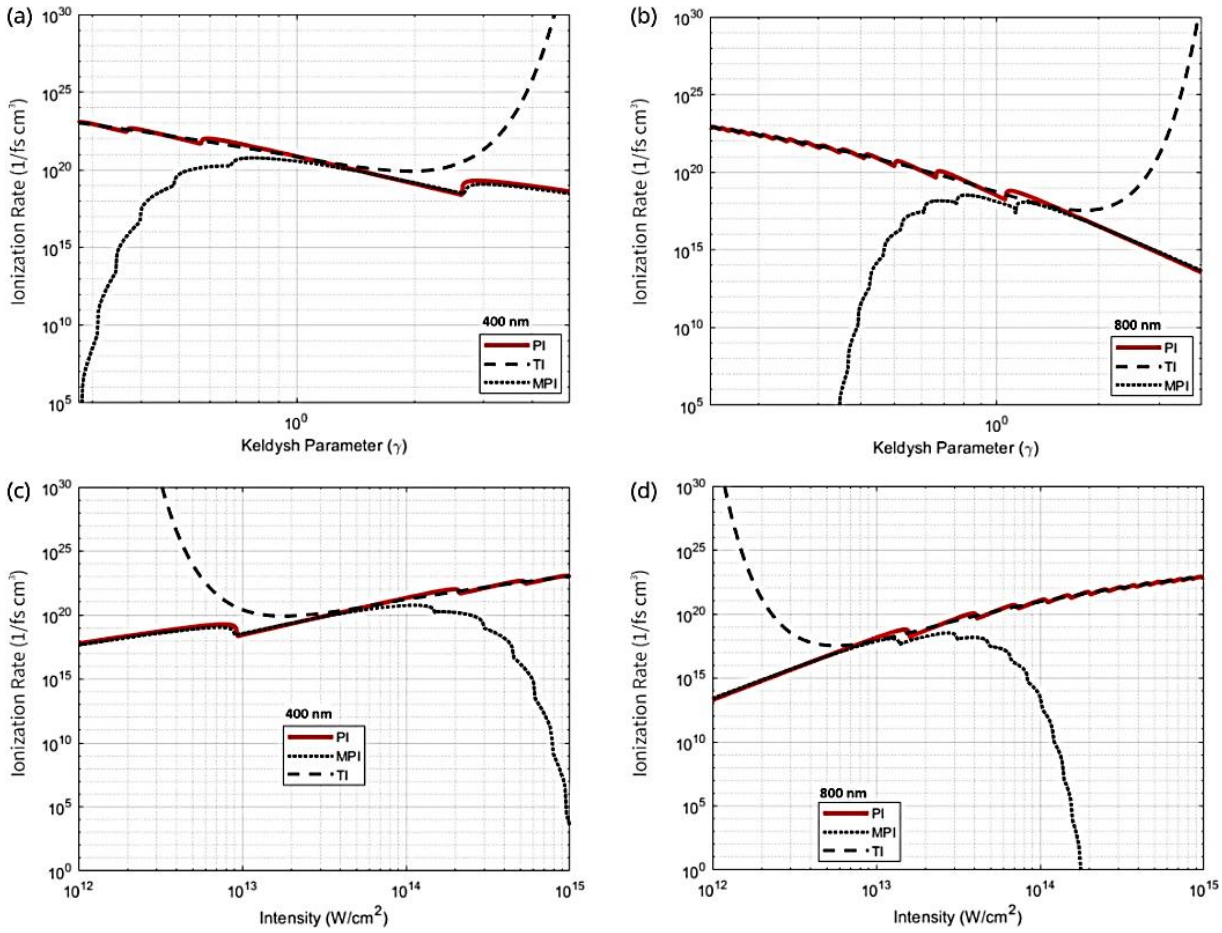

Figure 1. Comparison of ionization rate components based on PI rate, W_{PI}, TI rate, W_{TI}, and MPI rate, W_{MPI}. Panels (a) and (b) show these ionization rates as functions of the γ parameter, ranging from 0.01 to 8.0, for laser wavelengths of 400 nm and 800 nm. Panels (c) and (d) depict the ionization rates versus laser intensity, I, spanning from 1×10^{12} W/cm^2 to 1×10^{15} W/cm^2, for the same laser wavelengths.

Cascade ionization rate

CI significantly enhances electron density following the initial generation of free electrons through the comprehensive PI process in LIP. This secondary ionization process is crucial for the development of plasma and significantly impacts the interaction of laser with matter. After free electrons are generated by PI, they gain additional kinetic energy through IB. In this process, electrons absorb energy from the oscillating electric field of the laser. This is crucial because it equips electrons with the kinetic energy necessary to initiate further ionization events upon collision with other atoms or molecules in the medium. This is known as impact ionization, where an electron, now energetic enough, collides with an atom and can ionize it, freeing more electrons. Each of these newly liberated electrons can continue the avalanche events, resulting in an exponential increase in the electron population. The mathematical

expression that describes the rate of CI includes several parameters that help understand how efficiently this process occurs:

$$W_{CI} = \frac{1}{1+\omega^2{\tau_m}^2}\left(\frac{e^2\tau_m}{cnm_e\varepsilon_0 I_p} I - \frac{m_e\omega^2\tau_m}{M}\right). \quad (6)$$

Here, ω represents the angular frequency of the laser, while τ_m denotes the mean free time between electron collisions, indicating the average interval between successive interactions with surrounding particles. For the conditions considered in this study, τ_m has a value of 1.35 fs. Furthermore, e represents the electron charge, $e = 1.602 \times 10^{-19}$ C, and c is the speed of light in vacuum, $c = 3 \times 10^8$ m/s. The refractive index of the medium, n, can be calculated using the Sellmeier equation (BERGE, 1984), as discussed in the previous subsection. The effective electron mass, m_e, is defined as $m_e = 1.2\, m_e^0$, where m_e^0 is the electron's rest mass, $m_e^0 = 9.11 \times 10^{-31}$ kg. The permittivity of free space is denoted by ε_0, with a value of $\varepsilon_0 = 8.85 \times 10^{-12}$ F/m. The ionization potential of water, I_p, is taken as 6.5 eV, reflecting the effective energy required to liberate an electron from the water-like tissues under laser irradiation (VOGEL AND NOACK, 2001). Additionally, M represents the average mass of a water molecule, $M = 3 \times 10^{-26}$ kg. Finally, I denotes the laser intensity, which plays a critical role in determining the energy delivered to the medium and, consequently, the ionization dynamics.

In the context of water-like tissues, the dynamics of laser interaction are fundamentally different from those in materials with a high concentration of defects (BLOEMBERGEN, 1974; KUCHEYEV AND DEMOS, 2003). Unlike solid materials where different defects can serve as seed electrons for initiating CI, water-like tissues exhibit a different kind of variability that impacts their response to laser pulses. When applying long laser pulses, the process of ionization doesn't rely on defects but rather on the heterogeneity of the tissue itself (LI *et al.,* 2016), which includes variations in cellular structure and the presence of different solutes. These components absorb laser energy and can lead to localized increases in electron density. Over extended exposure times, this can result in both thermal and photochemical changes that progressively lower the threshold for tissue damage (DENTON *et al.,* 2024). This effect makes tissues with varied compositions more susceptible to breakdown at lower laser intensities compared to more homogeneous tissues. Determining the precise LIB thresholds in such cases is challenging due to the interplay of tissue components and their varied responses to laser energy. Conversely, when dealing with shorter laser pulses, particularly those in the fs range, the influence of these heterogeneous elements is greatly diminished. Instead, the primary driver of ionization is the tissue's absorption properties. This shift means that ionization under short pulses is less dependent on tissue composition and more reliant on the immediate and intense energy delivery characteristic of these pulses (RADOSEVIC *et al.,* 2021). Here mentioned type of ionization, often referred to as self-seeded due to its initiation by the laser energy itself rather than pre-existing free electrons, allows for more predictable and controlled interactions (NOACK AND VOGEL, 1999; FAN *et al.,* 2002; MANRIQUE *et al.,* 2024). It minimizes the thermal effects that are more prominent with longer pulses and focuses on precise, localized PI. This predictability is particularly important in medical applications where precise targeting and minimal collateral damage are essential.

RESULTS AND DISCUSSION

In this section, we delve into the results of our numerical study, which was conducted to explore the dynamics of LIB in water-like tissue media. The simulation is carried out to replicate the experimental conditions reported by (JIAO AND GUO, 2012; WANG *et al.*, 2015; LINZ *et al.*, 2016; MARTIN AND BEN-YAKAR, 2016; AKAMATSU *et al.*, 2024), employing the Runge-Kutta fourth-order technique with an adaptive time step to ensure precise computational

accuracy when solving Eq. (1) (ALI *et al.*, 2024). Our study focuses on the interaction of laser beams with wavelengths of 400 nm (Fig. 2) and 800 nm (Fig. 3), examining a spectrum of ultra-short pulse durations ranging from 1 fs to 150 fs. These wavelengths were selected due to their relevance in biomedical applications: 400 nm corresponds to visible violet light with strong absorption characteristics in biological tissues, whereas 800 nm lies within the near-infrared window, allowing deeper tissue penetration with reduced scattering and absorption. The pulse peak intensity considered in this study is fixed to the value of 5×10^{16} W/m^2. To place these conditions in context, it is important to note that while this value represents a typical experimental condition for LIB in water-like tissue, the electron dynamics and ionization processes are expected to vary with changes in peak intensity. At lower intensities, the rate of PI and subsequent CI would decrease, resulting in lower electron densities and slower plasma formation. Conversely, at higher intensities, the processes would be enhanced, potentially leading to earlier onset of ionization and higher final electron densities, which could approach the critical density for optical breakdown. Therefore, the presented results should be understood as representative of this specific intensity regime. Building on this foundation, by assigning the specific ionization processes that initiate LIB, we were able to perform calculations that highlight the temporal evolution of electron density across the selected pulse durations at 400 nm (see Fig. 2). To provide a clear comparative analysis, the results for four distinct pulse durations - 1 fs (Fig. 2(a)), 50 fs (Fig. 2(b)), 100 fs (Fig. 2(c)), and 150 fs (Fig. 2(d)) - are presented and analysed. Each of these figures features a comparison between the Gaussian laser pulse profile, $I(t)$, and the temporal evolution of electron density, $\rho(t)$, reflecting how the electron dynamics respond to the laser excitation. Specifically, the figures show: (i) total electron density, represented in black solid lines, indicating the cumulative effect of both PI and CI on electrons generation, as well as relaxation time, as governed by Eq. (1), $d\rho/dt = W_{PI} + W_{CI} \cdot \rho - W_R \cdot \rho$; (ii) PI density, shown in red solid lines, which isolates the contribution from PI alone, $d\rho/dt = W_{PI}$, providing insight into the initial electrons generation mechanism before any amplification effects from CI take place. As the laser pulse reaches its peak intensity, we observe a rapid increase in electron density in each panel in Fig. 2. This is primarily driven by PI, where photons with sufficient energy ionize the water-like tissue by exciting electrons from the valence to the conduction band. The quick rise in electron density corresponding almost directly with the Gaussian laser pulse's peak suggests that PI is the dominant mechanism during the initial phase of the pulse (YANG *et al.,* 2023). After peaking, the electron density stabilizes instead of decaying quickly, indicating a dynamic equilibrium between electron generation and loss. This stabilization points to an effective balance where the newly generated electrons through PI are both supplemented and sustained by avalanche processes. Therefore, CI, driven by the electrons' interactions with the material under the continuing influence of the laser field, leads to secondary electrons generation, thereby augmenting the initial population created by PI. As we extend the pulse duration from 1 fs to 150 fs, the influence of CI becomes increasingly significant. This is in accordance with the results presented by (HAMMER *et al.,* 1996; SARAPE-TUDORAN *et al.*, 2006; LINZ *et al.*, 2016). At the shortest pulse of 1 fs, the interaction time is insufficient for CI to substantially affect the electron density, which remains around 3.5×10^{11} 1/cm^3, closely reflecting the output solely from PI. Here, the high peak intensity and extremely short interaction time allow electrons to be liberated by photon absorption almost instantaneously, with minimal contribution from secondary processes. However, with a pulse duration increase to 50 fs, CI's impact becomes more pronounced, enhancing the electron density from PI's contribution of 1.8×10^{16} 1/cm^3 to a combined total of 2.4×10^{17} 1/cm^3. This increase is not merely additive but multiplicative, as seen from the electron densities increasing disproportionately with time. The reason lies in the nature of CI, where the initial electrons generated by PI gain enough kinetic energy via interactions with the laser field, to ionize other atoms or molecules. This leads to an avalanche effect, where one ionization event triggers several others, thereby exponentially increasing the electron density.

With 100 fs and 150 fs pulses, the electron density growth due to CI is even more pronounced. For a 100-fs pulse, while PI contributes $3.5 \times 10^{16}\ 1/\mathrm{cm}^3$, CI amplifies this to $1.3 \times 10^{19}\ 1/\mathrm{cm}^3$. At 150 fs, the PI-induced density of $5.3 \times 10^{16}\ 1/\mathrm{cm}^3$ escalates dramatically to $7.7 \times 10^{20}\ 1/\mathrm{cm}^3$ due to CI.

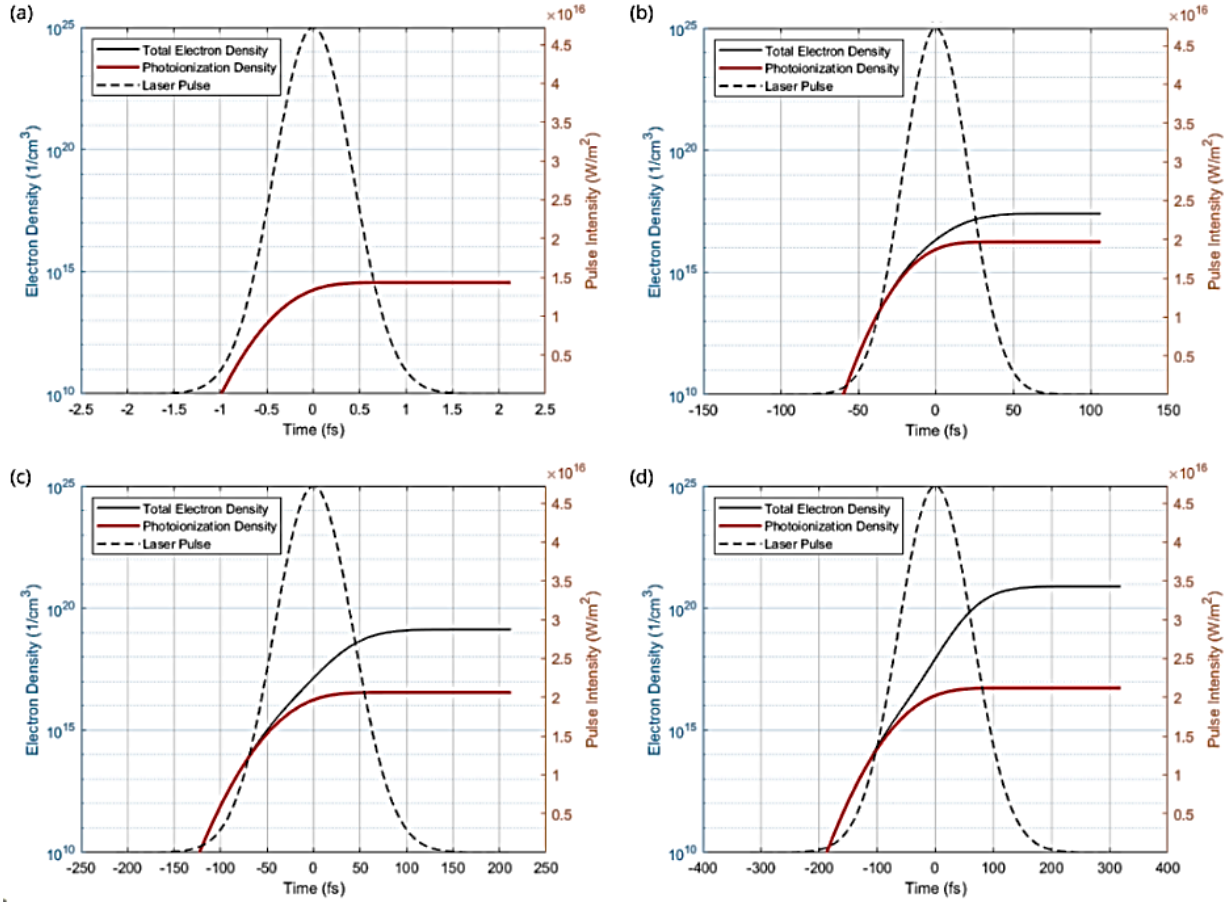

Figure 2. Temporal dynamics of electron density for laser pulses at 400 nm wavelength with varying pulse durations: (a) 1 fs, (b) 50 fs, (c) 100 fs, and (d) 150 fs. Each panel presents the Gaussian laser pulse profile, $I(t)$ (dashed line), and the resulting photoionization density (red solid line) alongside the total electron density (black solid line), with dual $y-$ axes for pulse intensity $[\mathrm{W/m}^2]$ and free-electron density $[1/\mathrm{cm}^3]$.

The substantial increase in electron density due to CI across longer pulse durations can be attributed to several factors. Extended pulse durations subject electrons to the laser's electric field for increased periods, which escalates their energy levels and subsequently enhances their probability of causing additional ionizations (HAMMER *et al.,* 1996; MIRZA *et al.,* 2016). Moreover, as pulse duration elongates, the tissue absorbs more energy, which not only elevates more electrons to excitable states but also allows sufficient time for these energized electrons to interact with their surroundings. This prolonged interaction time is crucial for facilitating more frequent impact ionization events. Additionally, the extended exposure under longer pulses increases the density of free electrons within the focus of the laser beam. This rise in electron density boosts the probability of electron-electron interactions, further driving the CI process. Such dynamics underline that while PI seeds the initial electron population, the prolonged laser exposure inherent to longer pulse durations dramatically enhances this population through CI. Finally, it is important to note that despite these increases, the electron densities remain well below the critical free-electron density threshold $\rho_{cr} = 6.9 \times 10^{21}\ 1/\mathrm{cm}^3$ for a 400 nm laser. This clearly indicates that, under the studied conditions, the tissue is

unlikely to undergo optical breakdown or sustain damage from laser irradiation. The electron densities achieved stay within a range that maintains the material's integrity, thus avoiding irreversible effects. Such control over electron generation is particularly important for medical applications, where ensuring the safety of biological tissues is paramount. In this way, the laser-tissue interaction remains in a non-destructive regime, making these findings relevant for clinical scenarios where precise and safe laser exposure is required.

In continuation of our exploration into LIB, Fig. 3 shifts the focus to the effects of laser pulses at an 800 nm wavelength. This wavelength is frequently chosen for applications requiring deeper tissue penetration, as it is less absorbed by biological chromophores, leading to distinctive interactions within the tissue (TUCHIN., 2016). By examining pulse durations of 1 fs (Fig. 3(a)), 50 fs (Fig. 3(b)), 100 fs (Fig. 3(c)), and 150 fs (Fig. 3(d)), we observe how the longer wavelength influences the electron dynamics compared to the 400 nm wavelength discussed previously.

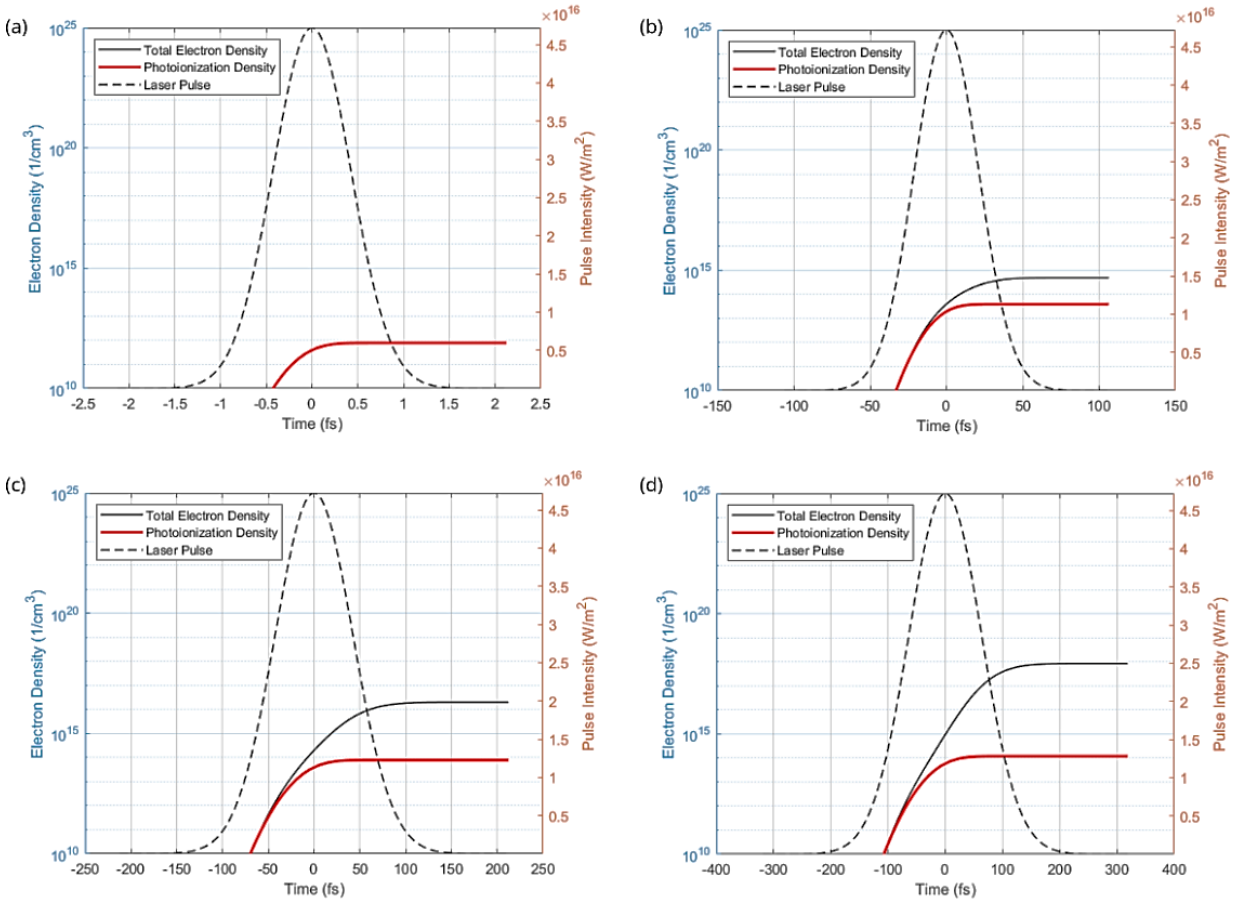

Figure 3. Temporal dynamics of electron density for laser pulses at 800 nm wavelength with varying FWHM durations: (a) 1 fs, (b) 50 fs, (c) 100 fs, and (d) 150 fs. Each panel presents the Gaussian laser pulse profile, $I(t)$ (dashed line), and the resulting photoionization density (red solid line) alongside the total electron density (black solid line), with dual $y-$ axes for pulse intensity $[\mathrm{W/m^2}]$ and free-electron density $[1/\mathrm{cm^3}]$.

While analysing Fig. 3, one can observe that as the 800 nm laser pulses reach their peak intensity, the electron density shows a rapid increase, akin to what was observed at 400 nm (see Fig. 2). This rise is similarly driven by PI, where the energy of the photons is sufficient to excite electrons across the bandgap from the valence to the conduction band. However, due to the lower photon energy at 800 nm, the ionization threshold is not as efficiently met as with the higher energy photons at 400 nm, which may slightly delay the onset of PI or reduce its efficiency per photon absorbed (see (HAMMER *et al.,* 1996; MIRZA *et al.,* 2016; TUCHIN., 2016)).

Despite this, once the electron density peaks, it stabilizes rather than decays quickly, indicating a dynamic equilibrium between electron generation and loss. This stabilization is indicative of an effective balance where the electrons generated through PI are supplemented and sustained by CI processes. The longer wavelength allows the laser's influence to penetrate deeper into the tissue before significant absorption occurs, extending the interaction volume and potentially affecting a larger volume of tissue. In terms of pulse duration effects at 800 nm, while the shortest 1 fs pulse does not allow for significant CI effects due to its very brief interaction time, resulting in electron density remaining at about $8.3 \times 10^{11}\ 1/\mathrm{cm}^3$, predominantly reflecting PI activity. As pulse duration increases to 50 fs and beyond, the role of CI becomes more significant. For example, at 50 fs, the electron density increases from a PI contribution of $3.9 \times 10^{13}\ 1/\mathrm{cm}^3$ to a total of $4.9 \times 10^{14}\ 1/\mathrm{cm}^3$ when including CI, showcasing a substantial multiplication effect. This continues to be more dramatic as the pulse duration extends further to 100 fs and 150 fs. At 100 fs, CI boosts the PI contribution of $7.9 \times 10^{13}\ 1/\mathrm{cm}^3$ to $1.9 \times 10^{16}\ 1/\mathrm{cm}^3$. By 150 fs, the PI-induced electron density of $1.2 \times 10^{14}\ 1/\mathrm{cm}^3$ is escalated to $8.5 \times 10^{17}\ 1/\mathrm{cm}^3$ due to CI. This increase in electron density at longer durations under 800 nm can be attributed to the longer interaction time provided by the deeper penetrating laser pulse, which sustains the electric field within the tissue for a longer period, thereby enhancing the kinetic energy of the electrons and increasing their probability of causing further ionizations. This extended interaction time, combined with the larger interaction volume at 800 nm, facilitates more frequent and sustained impact ionization events, enhancing the overall efficiency of the CI process. The deeper penetration of the 800 nm laser not only allows for a more extended interaction with the tissue but also reduces the rate of energy absorption per unit depth, which means that the energy is distributed over a larger volume, potentially reducing thermal effects while still achieving effective ionization (VOGEL AND VENUGOPALAN, 2003; TUCHIN, 2016; YANG *et al.,* 2023).

CONCLUSION

In this study, we have analysed the interactions of ultra-short laser pulses with water-like tissues, focusing on how variations in pulse durations influence primary ionization mechanisms - PI and CI. Our numerical simulations demonstrate that shorter pulses primarily drive PI due to their intense peak power and brief interaction times, effectively generating initial seed electrons. As pulse durations extend to 150 fs, these seeds undergo significant multiplication through CI, markedly enhancing electron density and intensifying LIB effects. Our findings corroborate existing research on transparent materials, asserting that longer pulses facilitate a more pronounced increase in electron density due to sustained CI effects. Additionally, by contrasting the effects at two different wavelengths, 400 nm and 800 nm, we observed that the longer wavelength allows for deeper tissue penetration with less absorption by biological chromophores. This characteristic leads to extended interaction volumes and times, particularly evident in longer pulse durations, which enhances the CI process significantly. At 800 nm, even though PI may initiate more slowly due to lower photon energy per pulse, CI profoundly increases electron density, particularly for pulse durations extending beyond 50 fs. In conclusion, the dynamic interplay between PI and CI, influenced by pulse duration and wavelength, dictates the behaviour of free electrons in laser-induced processes in water-like tissues. By exploring this interplay, we can enhance the precision and outcomes of laser applications in fields requiring control over material interactions at the microscopic level. These findings offer practical guidance for optimizing pulse duration and wavelength selection in medical laser treatments and material processing. Careful adjustment of these parameters can improve treatment efficacy while minimizing damage to surrounding tissues or materials, highlighting the relevance of our study beyond theoretical insights.

Acknowledgments

Authors would like to acknowledge the support received from the Science Fund of the Republic of Serbia, #GRANT 6821, Atoms and (bio) molecules-dynamics and collisional processes on short time scale - ATMOLCOL. Our appreciation also goes to the Serbian Ministry of Education, Science and Technological Development (Agreement No. 451-03-136/2025-03/ 200122). H. Delibašić Marković would also like to express gratitude to COST Actions CA21159 - "Understanding interaction of light with biological surfaces: possibility for new electronic materials and devices" for their support and CA22148 - "An international network for Non-linear Extreme Ultraviolet to hard X-ray techniques (NEXT)".

References:

[1] AKAMATSU, K., ENDO, T., AKAGI, H., KONO, H. AND ITAKURA, R. (2024): Specificity of DNA damage formation induced by femtosecond near-infrared laser filamentation in water. *Journal of Photochemistry and Photobiology B: Biology*, **258:** 112994. doi: 10.1016/j.jphotobiol.2024.112994.

[2] ALI, A.J., ABBAS, A.F. AND ABDELHAKEM, M.A. (2024): Comparative Analysis of Adams-Bashforth-Moulton and Runge-Kutta Methods for Solving Ordinary Differential Equations Using MATLAB. *Mathematical Modelling of Engineering Problems*, **11**(3). doi: 10.18280/mmep.110307.

[3] BERGE, T. (1984): *Applied Optics*, **23**(24): 4477–4485.

[4] BLOEMBERGEN, N. (1974): Laser-induced electric breakdown in solids. *IEEE Journal of Quantum Electronics*, **10**(3): 375–386. doi: 10.1109/JQE.1974.1068132.

[5] CHRISTENSEN, B.H., BALLING, P. (2009): Modeling ultrashort-pulse laser ablation of dielectric materials. *Physical Review B - Condensed Matter and Materials Physics*, **79** (15): 155424. doi: 10.1103/PhysRevB.79.155424.

[6] DELIBASIC, H., PETROVIC, V. AND PETROVIC, I. (2020): Laser breakdown in water induced by λ=532 nm nanosecond pulses: Analytical calculation of the number density of free electrons. *Journal of the Physical Society of Japan*, **89**(11): 114501. doi: 10.7566/JPSJ.89.114501.

[7] DELIBASIC, H., PETROVIC, V., PETROVIC, I. (2018): The effects of the perturbated ionization potential and the magnetic component on the relativistic transition rate. *Kragujevac Journal of Science*, **40**: 2332. doi: 10.5937/KgJSci1840023D.

[8] DELIBASIC, H., PETROVIC, V., PETROVIC, I., MOLPECERES, C., LAUZURICA, S. (2021): Numerical modeling of plasma formation in skin tissues induced by nanosecond pulsed laser. *The European Physical Journal D*, **75** (5): 155. doi: 10.1140/epjd/s10053-021-00170-z.

[9] DENTON, M.L., CLARK III, C.D., NOOJIN, G.D., WEST, H., STADICK, A., KHAN, T. (2024): Unified modeling of photothermal and photochemical damage. *Frontiers in Ophthalmology*, **4**: 1408869. doi: 10.3389/fopht.2024.1408869.

[10] DU, D., LIU, X., KORN, G., SQUIER, J., MOUROU, G. (1994): Laser-induced breakdown by impact ionization in SiO2 with pulse widths from 7 ns to 150 fs. *Applied physics letters*, **64**(23): 3071-3073. doi: 10.1063/1.111350.

[11] FAN, C.H., SUN, J., LONGTIN, J.P. (2002): Breakdown threshold and localized electron density in water induced by ultrashort laser pulses. *Journal of Applied Physics*, **91**(4): 2530-2536. doi: 10.1063/1.1433929.

[12] FANG, Q., HU, X.H. (2004): Modeling of skin tissue ablation by nanosecond pulses from ultraviolet to near-infrared and comparison with experimental results. *IEEE Journal of Quantum Electronics*, **40** (1): 69–77. doi: 10.1109/JQE.2003.820837.

[13] FU, Y.Z., ZHAO, S.F., ZHOU, X.X. (2012): Multiphoton and tunneling ionization of atoms in an intense laser field. *Chinese Physics B*, **21**(11): 113101. doi: 10.1088/1674-1056/21/11/113101.

[14] GRUZDEV, V. (2014): Fundamental mechanisms of laser damage of dielectric crystals by ultrashort pulse: ionization dynamics for the Keldysh model. *Optical Engineering*, **53**(12): 122515. doi: 10.1117/1.OE.53.12.122515.

[15] HAMAM, K.A., GAMAL, Y.E.D. (2018): Numerical analysis of breakdown dynamics dependence on pulse width in laser-induced damage in fused silica: Role of optical system. *Results in Physics*, **9**: 725-733. doi: 10.1016/j.rinp.2018.03.042.

[16] HAMMER, D.X., THOMAS, R.J., NOOJIN, G.D., ROCKWELL, B.A., KENNEDY, P.K., ROACH, W.P. (1996): Experimental investigation of ultrashort pulse laser-induced breakdown thresholds in aqueous media. *IEEE Journal of Quantum Electronics*, **32** (4): 670–678. doi: 10.1109/3.488842.

[17] HAN, J.H., MOON, Y., LEE, J.J., CHOI, S., KIM, Y.C., JEONG, S. (2015): Differentiation of cutaneous melanoma from surrounding skin using laser-induced breakdown spectroscopy. *Biomedical Optics Express*, **7** (1): 57–66. doi: 10.1364/BOE.7.000057.

[18] https://refractiveindex.info/ Accessed 25 February 2025.

[19] JIAO, J. AND GUO, Z. (2012): Analysis of plasma-mediated ablation in aqueous tissue. *Applied surface science*, **258**(17): 6266-6271. doi: 10.1016/j.apsusc.2012.03.019.

[20] KELDYSH, L.V. (1964): Ionization in the field of a strong electromagnetic wave. *Zhurnal Eksperimental'noi i Teoreticheskoi Fiziki*, **47**.

[21] KENNEDY, P.K. (1995): A first-order model for computation of laser-induced breakdown thresholds in ocular and aqueous media. I. Theory. *IEEE Journal of Quantum Electronics*, **31**(12): 2241-2249. doi: 10.1109/3.477753.

[22] KUCHEYEV, S.O., DEMOS, S.G. (2003): Optical defects produced in fused silica during laser-induced breakdown. *Applied Physics Letters*, **82**(19): 3230-3232. doi: 10.1063/1.1573364.

[23] LI, Y., GECEVICIUS, M. AND QIU, J. (2016): Long persistent phosphors—from fundamentals to applications. *Chemical Society Reviews*, **45**(8): 2090-2136. doi: 10.1039/C5CS00582E.

[24] LINZ, N., FREIDANK, S., LIANG, X.X., VOGEL, A. (2016): Wavelength dependence of femtosecond laser-induced breakdown in water and implications for laser surgery. *Physical Review B*, **94** (2): 024113. doi: 10.1103/PhysRevB.94.024113.

[25] LINZ, N., FREIDANK, S., LIANG, X.X., VOGEL, A. (2025): Laser-induced plasma formation and cavitation in water: from nanoeffects to extreme states of matter. arXiv preprint arXiv:2501.11029. doi: 10.48550/arXiv.2501.11029.

[26] MANRIQUE, J., GARRIDO, P., VELASCO, J. (2024): Laser-induced breakdown spectroscopy in biological samples: A review of experiments with soft tissues. *Atoms*, **12**(4): 21. doi: 10.3390/atoms12040021.

[27] MARTIN, C. AND BEN-YAKAR, A. (2016): Determination of scattering properties and damage thresholds in tissue using ultrafast laser ablation. *Journal of biomedical optics* **21**(11): 115004-115004. doi: 10.1117/1.JBO.21.11.115004.

[28] MIRZA, I., BULGAKOVA, N.M., TOMÁŠTÍK, J., MICHÁLEK, V., HADERKA, O., FEKETE, L., MOCEK, T. (2016): Ultrashort pulse laser ablation of dielectrics: Thresholds, mechanisms, role of breakdown. *Scientific reports*, **6**(1): 39133. doi: 10.1038/srep39133.

[29] NOACK, J., VOGEL, A. (1999): Laser-induced plasma formation in water at nanosecond to femtosecond time scales: calculation of thresholds, absorption coefficients, and energy density. *IEEE Journal of Quantum Electronics*, **35**(8): 1156-1167. doi: 10.1109/3.777215.

[30] NUZZO, V., SAVOLDELLI, M., LEGEAIS, J.M., PLAMANN, K. (2010): Self-focusing and spherical aberrations in corneal tissue during photodisruption by femtosecond laser. Journal of Biomedical Optics, **15** (3): 038003. doi: 10.1117/1.3455507.

[31] PETROVIĆ, V. AND DELIBAŠIĆ, H. (2019): Improved treatment of the photoionization process in the laser induced optical breakdown in the laser tissue. *UPB Scientific Bulletin, Series A: Applied Mathematics and Physics*, **81**(9): 287-300.

[32] POPOV, V.S. (2004): Tunnel and multiphoton ionization of atoms and ions in a strong laser field. *Physics-Uspekhi*, **47**(9): 855. doi: 10.1070/PU2004v047n09ABEH001812.

[33] RADOSEVIC, A., PRIETO, D., BURDÍO, F., BERJANO, E., PRAKASH, P., TRUJILLO, M. (2021): Short pulsed microwave ablation: computer modeling and ex vivo experiments. *International Journal of Hyperthermia*, **38**(1): 409-420. doi: 10.1080/02656736.2021.1894358.

[34] SACCHI, C.A. (1991): Laser-induced electric breakdown in water. *Journal of the Optical Society of America B*, **8**(2): 337-345. doi: 10.1364/JOSAB.8.000337.

[35] SAJJADI, A.Y., MITRA, K. AND GUO, Z. (2013): Thermal analysis and experiments of laser-tissue interactions: a review. *Heat Transfer Research*, **44**(3-4). doi: 10.1615/HeatTransRes.2012006425.

[36] SALEHI, A., PATURU, M.R., PATEL, B., CAIN, M.D., MAHLOKOZERA, T., YANG, A.B., LIN, T.H., LEUTHARDT, E.C., YANO, H., SONG, S.K., KLEIN, R.S. (2020): Therapeutic enhancement of blood–brain and blood–tumor barriers permeability by laser interstitial thermal therapy. *Neuro-Oncology Advances*, **2** (1): vdaa071. doi: 10.1093/noajnl/vdaa071.

[37] SARPE-TUDORAN, C., ASSION, A., WOLLENHAUPT, M., WINTER, M., BAUMERT, T. (2006): Plasma dynamics of water breakdown at a water surface induced by femtosecond laser pulses. *Applied Physics Letters*, **88** (26). doi: 10.1063/1.2217158.

[38] SCHAFFER, C.B., NISHIMURA, N., GLEZER, E.N., KIM, A.M.T., MAZUR, E. (2002): Dynamics of femtosecond laser-induced breakdown in water from femtoseconds to microseconds. *Optics Express*, **10** (3): 196–203. doi: 10.1364/OE.10.000196.

[39] TUCHIN, V. (2016): Tissue optics and photonics: Light-tissue interaction II. *Journal of Biomedical Photonics & Engineering,* **2**(3): 030201. doi: 10.18287/JBPE16.02.030201.

[40] VOGEL, A. AND VENUGOPALAN, V. (2003): Mechanisms of pulsed laser ablation of biological tissues. *Chemical reviews*, **103**(2): 577-644. doi: 10.1021/cr010379n.

[41] VOGEL, A., NOACK, J. (2001): Numerical simulation of optical breakdown for cellular surgery at nanosecond to femtosecond time scales. In *European Conference on Biomedical Optics*, 4433_70. doi: 10.1364/ECBO.2001.4433_70.

[42] WANG, H., ZHANG, W., LADIKA, D., YU, H., GAILEVIČIUS, D., WANG, H., PAN, C.F., NAIR, P.N.S., KE, Y., MORI, T., CHAN, J.Y.E. (2023): Two-photon polymerization lithography for optics and photonics: fundamentals, materials, technologies, and applications. *Advanced Functional Materials*, **33**(39): 2214211. doi: 10.1002/adfm.202214211.

[43] WANG, J., SCHUELE, G. AND PALANKER, D. (2015): Finesse of transparent tissue cutting by ultrafast lasers at various wavelengths. *Journal of Biomedical Optics*, **20**(12): 125004-125004. doi: 10.1117/1.JBO.20.12.125004.

[44] WANG, R., ZHANG, Q., LI, D., XU, S., CAO, P., ZHOU, Y., CAO, W., LU, P. (2019): Identification of tunneling and multiphoton ionization in intermediate Keldysh parameter regime. *Optics Express*, **27**(5): 6471-6482. doi: 10.1364/OE.27.006471.

[45] WEN, S.B., LY, K. (2019): Direct numerical simulation of laser induced breakdown and the associated micro-cavitation in a bio-tissue. *International Journal of Heat and Mass Transfer*, **131**: 873–889. doi: 10.1016/j.ijheatmasstransfer.2018.11.088.

[46] YANG, Z., ZHANG, C., YING, K., LI, Q., ZHANG, H., ZHANG, H., LU, J. (2024): Transient optical properties change and dense plasma dynamics during water breakdown induced by ultrashort laser pulses. *Physics of Plasmas*, **31** (5). doi: 10.1063/5.0203879.

[47] YANG, Z., ZHANG, C., ZHANG, H., LU, J. (2023): Transient electron temperature and density changes in water breakdown induced by femtosecond laser pulses. *Optics Communications*, **546**:129803. doi: 10.1016/j.optcom.2023.129803.